Numerical Gas Flow and Heat Transfer Simulation in the ASM Epsilon 2000 CVD Reactor for Pure Boron Deposition

Vahid Mohammadi, Saeide Mohammadi, Siva Ramesh and Stoyan Nihtianov

Abstract – **The gas flow and heat transfer in the ASM Epsilon 2000 CVD (chemical vapor deposition) reactor is numerically simulated for several reactor conditions by using commercial Gambit and FLUENT$^{©}$ software for pure boron (PureB) depositions at 700°C. The conditions for the gas flow rates are 25 slm, 20 slm and 15 slm , while the susceptor rotation is changed between 0 rpm, 10 rpm, 20 rpm and 35 rpm at atmospheric (ATM) ambient pressure. The results of this simulation are employed to develop an analytical kinetic model to predict deposition rate of PureB-layers.**

Keywords – **FLUENT, CFD, heat transfer, pure boron (PureB), CVD**

I. INTRODUCTION

The Chemical Vapor Deposition (CVD) process is considered as one of the most important thin film deposition techniques used in the silicon-based integrated circuit technology, because of its versatility; allowing thickness, structural and composition control, good uniformity and high deposition rates [1]. This study, however, will emphasize the gas flow and heat transfer in the ASM Epsilon 2000 CVD reactor for deposition of the pure boron (PureB) layers using diborane gas. PureB-layers are used in the fabrication of semiconductor devices for an increasing number of applications. In the as-deposited form the PureB-layer forms a highly-doped p^+ region on Si that can be used as the p^+ region of nanometer-shallow, low-leakage p^+n junctions [2]. This has found application in detectors for low penetration-depth beams [3-5] and other potential applications including UV sensitive photodiodes for integration in front-end CMOS [5].

Several simulation models accounting for complex flow patterns, as well as heat and mass transfer in different type of CVD reactors have been developed. For example, a set of simulations for 2D-and 3D transport phenomena, flow effects and heat transfer are performed in horizontal CVD reactors with different geometries [6, 7]. References [8-10] present numerical simulations for PECVD, RDCVD and barrel type CVD reactors, respectively. An aerosol dynamic simulation is performed by S. Kommu et.al. [11] to study the role of particle nucleation, growth and transport in ASM Epsilon One CVD reactor with a totally different reactor geometry than ASM Epsilon 2000.

In this paper, the gas flow and the heat transfer in the

V. Mohammadi, S. Ramesh and S. Nihtianov are with the Department of Microelectronics, Delft University of Technology, Delft, The Netherlands. S. Mohammadi is with the Department of Mechanical Engineering, Isfahan University of Technology.

Email (correspond author): V.Mohammadi@tudelft.nl

ASM Epsilon 2000 CVD reactor is numerically simulated by using Gambit software and commercial CFD package of FLUENT$^{©}$ for PureB depositions at 700°C with different reactor conditions i.e. the atmospheric (ATM) pressure, susceptor rotation speeds of 0 rpm, 10 rpm, 20 rpm and 35 rpm, and gas flow rates of 25 slm, 20 slm and 15 slm. The results of this simulation are employed to develop an analytical kinetic model to predict the deposition rate of PureB-layers [12]. This model takes many of the important factors into account. These include the mechanisms by which the diborane species diffuses through the stationary boundary layer formed over the wafer as well as the gas phase interactions and the related surface reactions [13]. To achieve this, the actual parabolic gas velocity and temperature gradient profiles in the reactor are employed to describe the deposition kinetics and the deposition chamber characteristics that determine the deposition rate over the non-rotating bare silicon wafer.

II. SYSTEM DESCRIPTION

In Fig. 1 a schematic illustration is shown of the ASM Epsilon 2000 CVD reactor geometry that is used in the simulation. The dimensions of the reactor are shown in the figure.
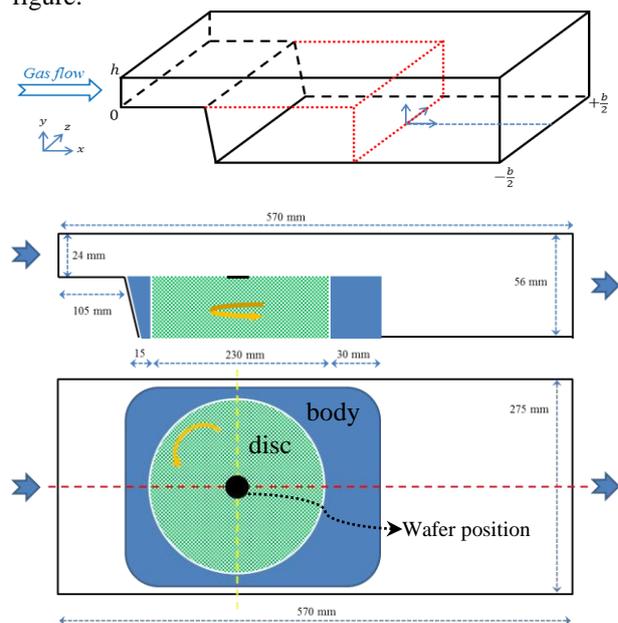

Fig. 1. Schematic of the ASM Epsilon 2000 CVD reactor geometry

In this system, the susceptor lies at the bottom of the chamber and consists of two parts; susceptor disc and body

as shown in Fig. 1. The wafer is placed in a packet located at the middle of the susceptor disc and rotated at a given speed depending on a recipe. The Body is the stationary part of the susceptor around the disc. The susceptor is heated up and held at deposition temperature through an assembly of lamps from top and bottom. Part of this heat is transferred to the gas flowing over the susceptor; whereas the temperature of the upper wall is much cooler than the susceptor. Moreover, we have assumed that the gases have room inlet temperature. The deposition conditions are chosen such that the reactant (B_2H_6) concentrations can be assumed to be much smaller than the concentration of the carrier gas (H_2). From this it follows that the gas flow and temperature profiles are completely determined by the physical constants of the carrier gas.

III. NUMERICAL SIMULATION

The mathematical model for the simulations can be described by the governing three-dimensional (3D) partial differential equations, i.e., the equations of conservation of mass (continuity equation), of momentum (Navier –Stokes equation), and of energy, as follows respectively:

$$\nabla \cdot \vec{u} = 0 \qquad (1)$$

$$\rho_0 \left(\frac{\partial \vec{u}}{\partial t} + \vec{u} \cdot \nabla \vec{u} \right) = -\nabla p + \mu \nabla^2 \vec{u} + \rho \vec{g} \qquad (2)$$

$$\rho_0 C_p \left(\frac{\partial T}{\partial t} + \vec{u} \cdot \nabla T \right) = k \nabla^2 T \qquad (3)$$

where $\vec{u}$ is the velocity vector. p, T, t and g represent: the pressure, the temperature, the time and an external force, respectively. Physical properties such as density (ρ), viscosity (μ), heat capacity (Cp), and thermal conductivity (k) are defined for hydrogen. Subscript 0 denotes the reference state. The buoyancy force is calculated by the Boussinesq approximation with the volume expansion coefficient (β) calculated from the ideal gas law, as follows:

$$\rho = \rho_0 (1 - \beta (T - T_0)) \qquad (4)$$

Simulations are performed using GAMBIT and FLUENT© software. The 3D geometry of Fig. 1 is first modeled in GAMBIT and meshed using the Cooper Scheme as an unstructured 3D meshing tool. The results can be seen in Fig. 2 with, in total, 180049 Hexahedral cells in the 3D domain.
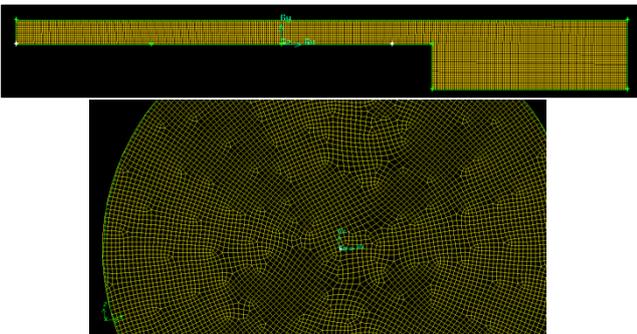

Fig. 2. Meshed structure (top) side view (bottom) susceptor disc.

Then the CFD package of FLUENT© is used to solve the equations for the steady state case and compute the results. The SIMPLE algorithm is used as a solver. The first-order upwind differencing scheme has been used to discretize momentum and energy terms and convergence criterion of 1×10^{-5} for continuity and velocity components, and of 1×10^{-6} for energy is considered as satisfactory. Simulations are then performed with the susceptor temperature taken as 700°C and with different disc rotating speeds of 0 rpm, 10 rpm, 20 rpm and 35 rpm and the gas flow rates of 25 slm, 20 slm and 10 slm which correspond to velocities of 6.1 cm/s, 5.1 cm/s and 3.8 cm/s respectively. In order to establish the efficacy of the susceptor system, full 3D simulations are carried out.

IV. RESULTS AND DISCUSSION

The uniformity of the PureB-layer deposited by this CVD reactor depends, on one hand, on the uniform distribution of substrate temperature and on the other hand, on the flow velocity patterns uniformity near the substrate.

Fig. 3 shows temperature distributions inside the reactor for different gas flow (slm) and susceptor rotation speed (rpm) conditions as specified in the figure. The distributions presented in (a), (b) and (c) are the 3D illustrations, 2D cross section of the middle plans in direction of the gas flow and perpendicular to the gas flow respectively.

At zero rpm (stationary susceptor) a thermal boundary layer created over the susceptor is clearly visible ("20 slm,0 rpm" b and c in Fig. 3). At this condition the temperature profile is also symmetrical in the perpendicular plan to the gas flow with a vertical gradient as can be seen in Fig. 3 "20 slm,0 rpm" (c). This condition is not desired due to a very narrow thermal boundary layer, with temperature of deposition over the susceptor, which significantly limits the number of active precursors for deposition. By rotating the susceptor the temperature distribution becomes more and more uniform and the thermal boundary layer expands vertically over the susceptor where the wafer is located. This can be seen by comparing the thermal distributions of Fig. 3 with different rpms at the same slm. It can be concluded that the temperature distribution becomes more homogenous at higher susceptor rotation speeds.

Fig. 4 shows the gas flow profiles determined by 3D numerical simulations for different rpms and slms as indicated in the figure. It can be seen that at zero rotation, the gas flow is laminar and dominated by forced convection. Rotation of the susceptor disc causes a gas rotation due to the frictional force between them and makes a cylindrical disturbance. This disturbance somehow facilitate the transportation of the reactant precursors to the substrate while at the same time introduces a gas velocity gradient over the substrate as can be seen in the images presented in Fig. 4 (b) and (c). This gradient is increased with increasing susceptor rotation speed. The direction of gas rotation and velocity gradient is clearly visible in Fig. 5 where the gas velocity vectors are presented. Beside cylindrical disturbance, the gas flow is still laminar and flowed with forced convection. Therefore intermingling due to free convection can be negligible. The return flow of heated gas occurring at the leading edge of the hot susceptor is also visible in all cases in Fig. 4. Gas-phase diffusion inside the reactor is investigated in ref. [12].

Investigating the images given in Fig. 4 result in the conclusion that the gas velocity over the susceptor disc is

mainly defined by rpm, while the gas flow (slm) can control the height of the stagnant gas-phase boundary layer as described in [12]. Both these parameters have an impact on the uniformity of PureB deposition.

V. CONCLUSION

Temperature distributions and gas velocity profiles are investigated inside the reactor for different conditions. It has been found that the gas flow (slm) controls the height of stagnant boundary layer and rotating the susceptor disc provides more homogenous temperature distribution while causing an increase in the gas velocity gradient over the susceptor which in turn can cause non-uniform deposition.

REFERENCES

[1] M.L. Hitchman, K.F. Jensen, Chemical Vapor Deposition: Principles and Applications. Academic Press, 1993.
[2] F. Sarubbi, et.al., *High effective Gummel number of CVD boron layers in ultrashallow p^+n diode configurations*, IEEE Trans. Electron Devices 57(6), pp. 1269-1278, 2010.
[3] L. Shi, et.al., *Electrical Performance Optimization of a Silicon-based EUV Photodiode With Near-theoretical Quantum Efficiency*, IEEE Transducers, pp. 48-51, 2011.
[4] A. Šakic, et al., *Versatile silicon photodiode detector technology for scanning electron microscopy with high-efficiency sub-5 keV electron detection*, IEDM 2010, p. 712.
[5] V. Mohammadi, et.al., *VUV/Low-Energy-Electron Si Photodiodes with Post-Metal 400°C PureB Deposition*, IEEE Electron Device Letters 34(12), pp. 1545-1547, 2013.
[6] C.R. Kleijn, et.al., *A study of 2-and 3-D transport phenomena in horizontal chemical vapor deposition reactors.* Chem. Eng. Science, 46(1), pp. 321-334, 1991.
[7] H.K. Moffat, et.al., *Three-Dimensional Flow Effects in Silicon CVD in Horizontal Reactors.* J. Electrochem. Soc. 135(2), pp. 459-471, 1988.
[8] A.N.R. da Silva, et.al., *Gas Flow Simulation in a PECVD Reactor.* ICCN 2002, pp. 360-363.
[9] G. Evand and R. Greif. *A numerical model of the flow and heat transfer in a rotating disk chemical vapor deposition reactor*, J. Heat Transfer 109, p. 928, 1987.
[10] H. Nabati and J. Mahmoudi. *Fluid flow and heat transfer simulation in a barrel type CVD reactor*. 49th SIMS 2008.
[11] S. Kommu, et.al., *Simulation of aerosol dynamics and transport in chemically reacting particulate matter laden flows. Part II: Application to CVD reactors.* Chem. Eng. Science 59(2), pp. 359-371, 2004.
[12] V. Mohammadi, et.al., *An Analytical Kinetic Model for Chemical-Vapor Deposition of Pure-Boron Layers from Diborane*, J. of Applied Physics 112(11), pp. 113501-10, Dec. 2012.
[13] V. Mohammadi, et.al., *Temperature Dependence of PureB-Layer Chemical-Vapor Depositions from Diborane*, Applied Physics Letter 101(11), pp. 111906-4, Sep. 2012.
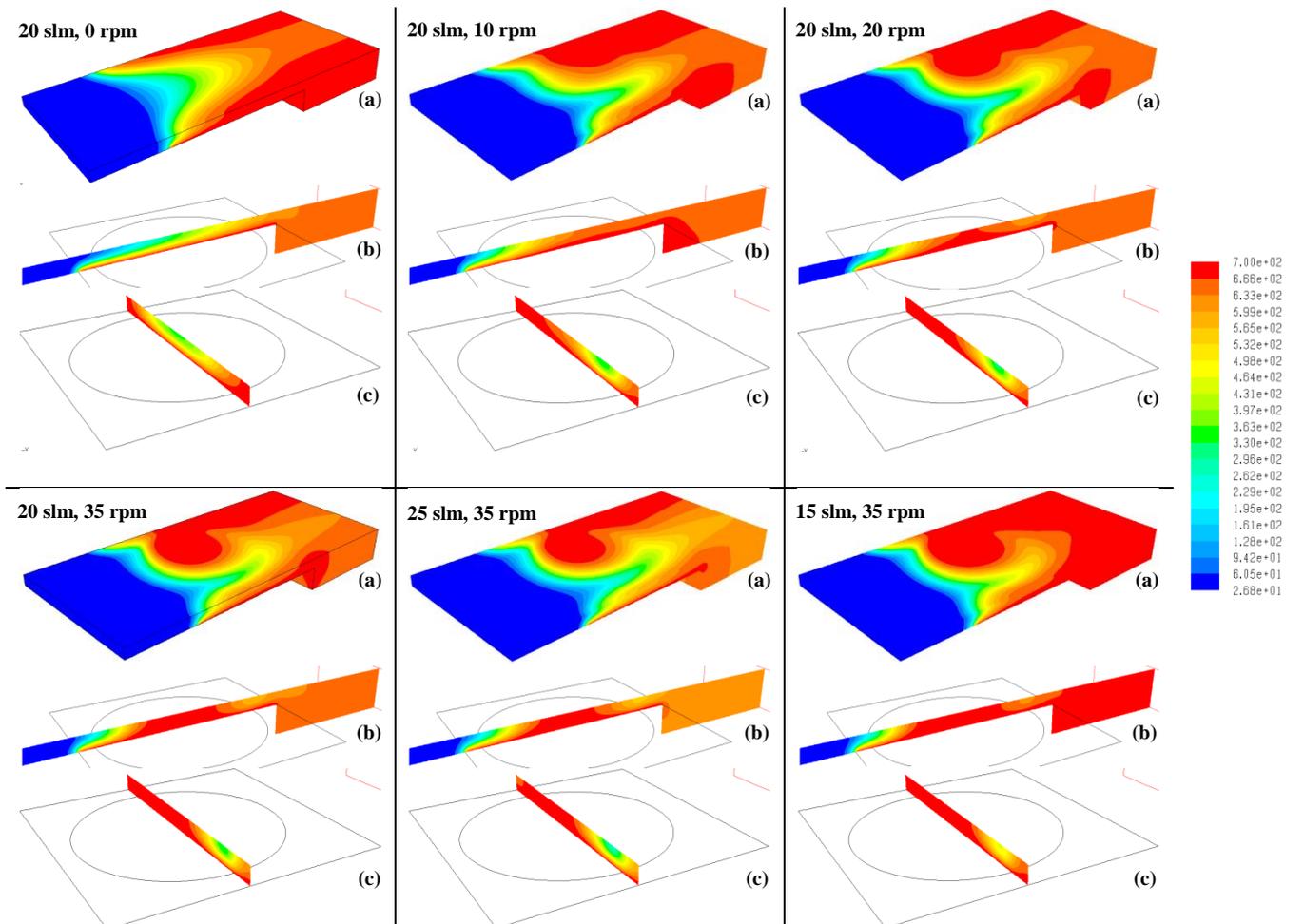
Fig. 3. (a) 3D and 2D middle plane, (b) in the direction of gas flow, and (c) perpendicular to the direction of the gas flow of the temperature distributions inside the reactor for different slm and rpm conditions, as indicated in the figure.
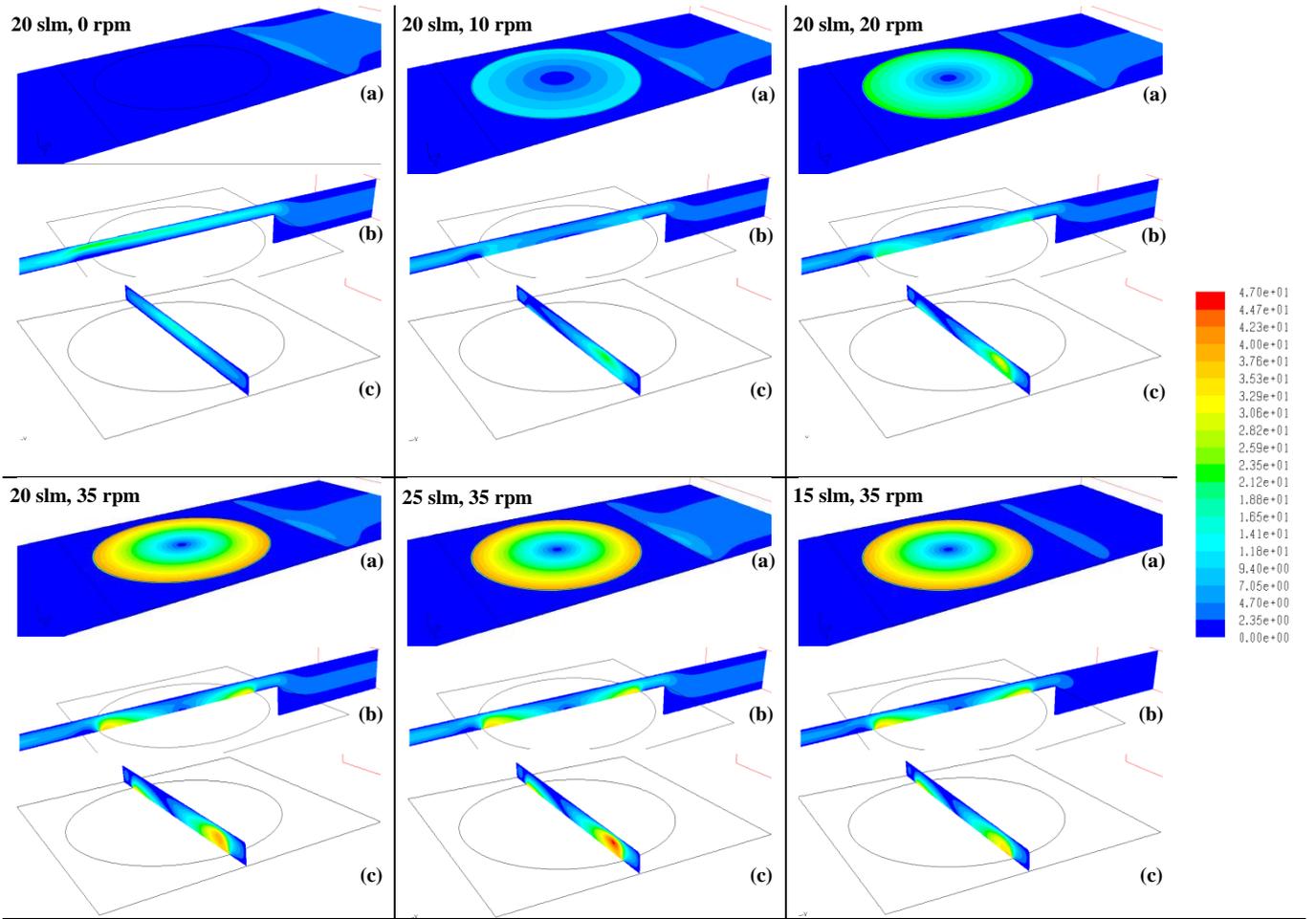
Fig. 4. (a) 3D and 2D middle plane, (b) in the direction of gas flow, and (c) perpendicular to the direction of the gas flow, of the gas velocity profiles inside the reactor, for different slm and rpm conditions as indicated in figure.
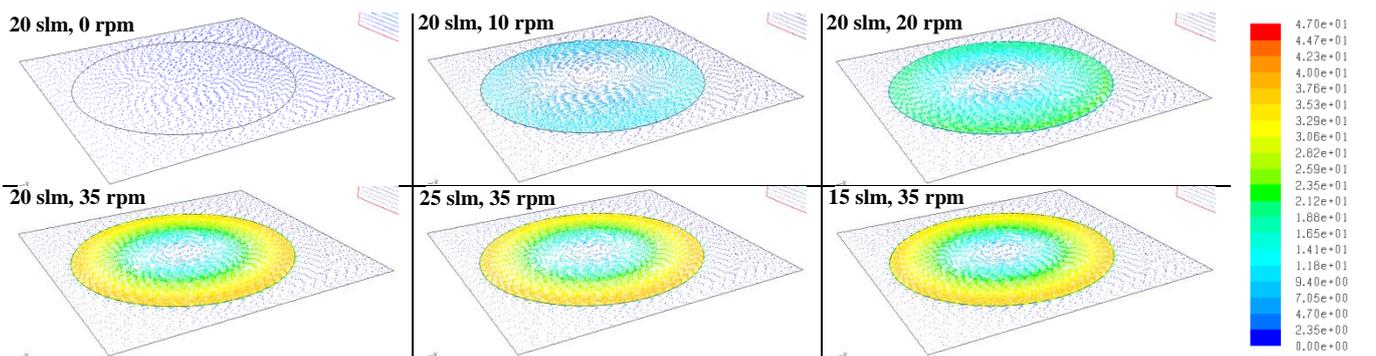

Fig. 5. Gas velocity vectors for different slm and rpm conditions as indicated in figure